molecular pharmaceutics

Article

Cite This: *Mol. Pharmaceutics* 2019, 16, 2912−2921

pubs.acs.org/molecularpharmaceutics

Incorporation of Nitroprusside on Silica Nanoparticles—A Strategy for Safer Use of This NO Donor in Therapy

Pedro M. Silva Filho,[†] Iury A. Paz,[§] Nilberto R. F. Nascimento,[‡] Cláudia F. Santos,[‡] Valdevane R. Araújo,[‡] Camila P. Aquino,[‡] T. S. Ribeiro,[∥] Igor F. Vasconcelos,[∥] Luiz G. F. Lopes,[§] Eduardo H. S. Sousa,*[,§] and Elisane Longhinotti*[,†]

[†]Departamento de Química Analítica e Físico-Química, Universidade Federal do Ceará, 60440-900 Fortaleza, Ceará, Brazil

[‡]Instituto Superior de Ciências Biomédicas, Universidade Estadual do Ceará, 60714-110 Fortaleza, Ceará, Brazil

[§]Departamento de Quımica Orgânica e Inorgânica, Universidade Federal do Ceará, Cx. Postal 6021, 60440-900 Fortaleza, Ceará, Brazil

[∥]Departamento de Engenharia Metalúrgica e de Materiais, Universidade Federal do Ceará, 60440-554 Fortaleza, Ceará, Brazil

Supporting Information

ABSTRACT: Silica-based nanoparticles have been developed as powerful platforms for drug delivery and might also prevent undesired side effects of drugs. Here, a fast method to synthesize positively charged mesoporous silica nanoparticles (ζ = 20 ± 0.5 mV, surface area = 678 m^2 g^{-1}, and 2.3 nm of porous size) was reported. This nanomaterial was employed to anchor sodium nitroprusside (SNP), a vasodilator drug with undesired cyanide release. A remarkable incorporation of 323.9 ± 7.55 μmol of SNP per gram of nanoparticle was achieved, and a series of studies of NO release were conducted, showing efficient release of NO along with major cyanide retention (ca. 64% bound to nanoparticle). Biological assays with mammalian cells showed only a slight drop in cell viability (13%) at the highest concentration (1000 μM), while SNP exhibited an LC_{50} of 228 μM. Moreover, pharmacological studies demonstrated similar efficacy for vasodilation and sGC-PKG-VASP pathway activation when compared to SNP alone. Altogether, this new SNP silica nanoparticle has great potential as an alternative for wider and safer use of SNP in medicine with lower cyanide toxicity.

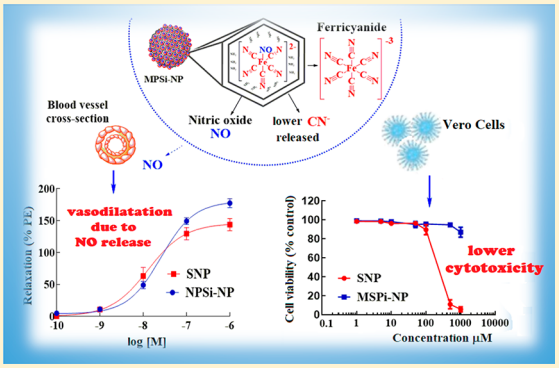

KEYWORDS: *nitric oxide delivery, silica nanoparticles, cyanide trapping, vasodilation, cytotoxicity*

INTRODUCTION

Sodium nitroprusside (SNP) has been used as a nitric oxide (NO) donor in medicine for several decades in cases of hypertension emergency because of its fast release of NO causing a fast drop in blood pressure.[1] Unfortunately, this compound requires coadministration of antidotes such as thiosulfate or hydroxocobalamin to minimize toxic issues caused by cyanide (CN^-) release.[1,2] In addition to that, SNP is highly hydrophilic and can decompose upon prolonged light irradiation. Interestingly, despite these issues, SNP is still widely used in clinical procedures,[1] which has called for a better strategy to prevent cyanide toxicity and expand its clinical use. So far, there are only a few potential iron-based nitric oxide donors that are cyanide-free,[3−8] but they are still far away from any clinical use. Nonetheless, even upon eventual clinical approval of those compounds, they might not even replace SNP in the same clinical application because of their biodistribution and rates of NO release. Then, any attempt to improve SNP properties might open many new opportunities for its safer use as well as repurposing its clinical application.

Nanomaterials have emerged as a powerful tools for incorporation and delivery of medicines into specific biological sites.[9−11] Thereby, these new nanomaterials could improve the therapeutic dosage of drugs, while minimizing their undesired side effects by driving the drugs toward a specific site of action.[12,13] Mesoporous silica nanoparticles (MSNs) have caught scientific attention because of their interesting properties such as high surface area, organized porous structure, and size (2−50 nm), providing a compatible environment for adsorption, encapsulation, and delivery of drugs. On the top of that, zeta potential and shape have also a significant influence in the proper use of this nanomaterial as a drug delivery system. The shape of the nanomaterial has also been explored using both spherical and nonspherical particles, where the latter seems to have superior features in many aspects of the drug delivery process.[14] In addition to that, MSNs have already

Received: January 24, 2019
Revised: May 10, 2019
Accepted: May 13, 2019
Published: May 13, 2019

DOI: 10.1021/acs.molpharmaceut.9b00110
Mol. Pharmaceutics 2019, 16, 2912−2921

a well-described chemistry and functionalization strategies that can be used as potential drug delivery platforms.[15−17]

Having those approaches in mind, a few groups have designed new materials based on silica to create a suitable environment for vasodilator drugs such as SNP or analogues while maintaining their capacity to release NO.[10,17] Farooq et al.[18] prepared an interesting material, where they incorporated SNP onto a fluorescent mesoporous silica matrix as a delivery system. In that study, ex vivo real-time vasodilator action of SNP on arterial vessels was reported for the first time. The authors showed the mesoporous silica worked as a vehicle to control NO delivery by releasing SNP in solution, which led to the relaxation of smooth muscle cells.[18] Unfortunately, their nanomaterial incorporated a quite limited amount of SNP and did not show evidence of retaining any cyanoferrate moieties, limiting its full application.

Here, we report a fast method to synthesize positively charged mesoporous silica nanoparticles, modified with amino groups (named MPSi−NH_2), using ultrasound. This MPSi−NH_2 material was used for a strong adsorption of the SNP complex, producing a new NO delivery system, named MPSi−NP. Our main goal was to ensure that only NO molecule is released from this nanomaterial, while the material could work to induce vasodilation in the aorta and pulmonary arteries in ex vivo studies. Additionally, this new nanosystem was investigated as a great trap for cyanide ions, a promising alternative to minimize SNP problems caused by cyanide toxicity.

MATERIALS AND METHODS

Chemicals. Materials used include sodium nitroprusside (≥99%, SNP, Merck), 3-aminopropyltriethoxysilane (≤98%, APTES, Sigma-Aldrich), tetraethyl orthosilicate (≤98%, TEOS, Sigma-Aldrich), ammonium hydroxide (28%, NH_4OH, Synth), ethanol (95%, EtOH, Dinâmica), and cetyltrimethyammonium bromide (≥99%, CTAB, VETEC). Physiological salt solution (PSS) was prepared using the following chemical composition [mM]: 119 NaCl, 4.7 KCl, 1.2 $MgSO_4·7H_2O$, 25 $NaHCO_3$, 1.17 KH_2PO_4, 0.03 $K_2EDTA·2H_2O$, 5.5 glucose, and 1.6 $CaCl_2·2H_2O$; pH 7.4. Potassium physiological salt solution (KPSS) was prepared using the following chemical composition [mM]: 78.2 NaCl, 60 KCl, 1.2 $MgSO_4·7H_2O$, 25 $NaHCO_3$, 1.17 KH_2PO_4, 0.03 $K_2EDTA·2H_2O$, 5.5 glucose, and 1.6 $CaCl_2·2H_2O$; pH 7.4.

Synthesis of Silica Nanoparticles Functionalized with Primary Amine (MPSi−NH_2). This procedure was adapted from the literature,[19] where, first, a solution of 100 mL of water containing 0.1 g of CTAB was prepared and maintained on ultrasound for 2 min with addition of 1 mL of concentrated ammonium hydroxide. Then, 10 mL of an alcohol solution containing 1 mL of TEOS and 10 mL of another alcohol solution containing 1 mL of APTES were added alternately into the CTAB solution. This mixture was left on ultrasound for ca. 15 min. Afterward, this material was washed several times with water, spun down, and, finally, redispersed in ethanol. The surfactant was removed by acid extraction using 0.5 g of the solid sample with 100 mL of an ethanol/hydrochloric acid mixture (99:1 v/v) by stirring for 16 h at room temperature. The CTAB-removed sample was spun down, washed with ethanol/water several times and, finally, twice with acetone, and dried for 24 h at 60 °C; the sample was named MPSi−NH_2.

Characterization of MPSi−NH_2. The morphology of the nanoparticles was investigated by scanning electron microscopy (SEM) measurements using an FEG Quanta 450 electron microscope equipped with an energy dispersive spectroscopy (EDS) Bruker QUANTAX system, coupled to the SEM microscope, using an acceleration voltage of 20 kV. Textural properties were studied by N_2 adsorption−desorption isotherms and measured on a Quantachrome Autosorb-1B instrument at the temperature of liquid nitrogen. All samples were degassed at 250 °C prior to the measurements. The specific surface area of the samples was calculated using the BET method. The pore size distribution was derived from the adsorption branches of the isotherms using the Barrett−Joyner−Halenda (BJH) method.[20] The zeta potential of the MPSi−NH_2 suspension at 0.5% (w/v) (in water) was measured, in triplicate, using a Zetasizer Nano ZS (Malvern Instruments Ltd., Worcestershire, United Kingdom). Infrared vibrational measurements were done from 4000 to 400 cm^{-1}, and samples were prepared as 3 wt % dispersions in KBr pellets in spectrophotometer ABB model FTLA 2000.

Preparation of Sodium Nitroprusside Anchored on MPSi−NH_2 (MPSi−NP). A 100 mg sample of MPSi−NH_2 was added to 20 mL of a 0.1 M concentration of nitroprusside (NP) in aqueous solution and stirred for 24 h at room temperature (protected from light). This material was spun down and washed three times, twice with water and once with acetone, and then dried at 30 °C for 24 h. The amount of the NP incorporated on MPSi−NH_2 was measured by spectrophotometry in a UV−Vis spectrophotometer Cary 5000 (Agilent). This analysis used 4 mg of MPSi−NP dissolved in 5 mL of 3 M NaOH solution, and the absorbance was measured at 398 nm. Quantification was carried out using a standard analytical curve of the free $[Fe(CN)_5NO_2]^{4-}$ complex,[21,22] prepared from 0.1 to 0.9 mM in 3 M NaOH solution.

NO Release. Experiments of NO release from MPSi−NP were monitored by changes in the characteristic NO absorption band in the infrared (IR) and/or UV−vis electronic spectra at different experimental conditions as described below as well as by using Griess assay.

Photochemical Release. *In Pellets of KBr.* NO release study was performed by dispersing ca. 3% (m/m) of MPSi−NP in KBr, which was then pressed to 10 Torr to make pellets. This pellet was exposed to blue LED (450−495 nm), and IR spectra were collected for 84 h.

In Aqueous Solution. This study was done employing 100 mg of MPSi−NP completely dispersed in 10 mL of water, which was irradiated with blue LED (450−495 nm) for 18 h. After that, MPSi−NP was spun down at 5000 rpm, washed with water, ethanol, and acetone, and then dried at 40 °C. The disappearance of a typical NO stretching band was noticed by IR analysis, and other changes werebshown by Mössbauer analysis in the solid material. Electronic spectra of the supernatants were taken.

Griess Assay. This assay was carried out using 1.4 mg of NPSi-NP and 9.5 mg of free SNP irradiated with blue LED light for 18 h in 10 mL of PBS. After these samples were spun down and filtrated (0.45 μm, Millex SLCR013NL), 5 mL of supernatant was diluted to 10 mL and mixed with 0.40 mL of Griess reagent. All quantitative measurements were done in duplicate, and a standard curve of nitrite was built employing the absorbance measured at 543 nm (R^2 = 0.997, ABS = $42.85[NO_2^-] - 0.098$).

Chemical Release Experiments. *Addition of Ascorbic Acid.* This measurement was carried out using 100 mg of

DOI: 10.1021/acs.molpharmaceut.9b00110
Mol. Pharmaceutics 2019, 16, 2912−2921

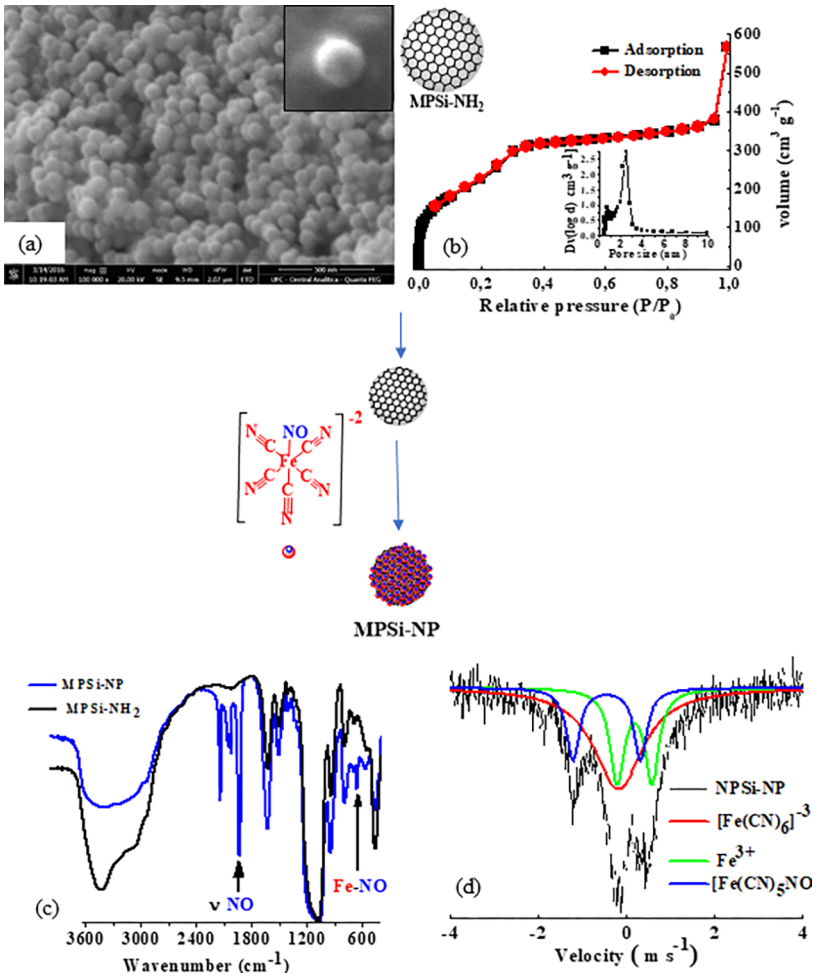

Figure 1. Nanoparticle characterizations. SEM analysis (a), N_2 adsorption−desorption for MPSi−NH_2 (b), FTIR spectrum for MPSi−NH_2 and MPSi−NP (c), and Mössbauer for MPSi−NP (d).

MPSi−NP dispersed in 10 mL of 8 mM ascorbic acid in PBS, which was kept stirring for 2 h. After that, MPSi−NP was spun down at 5000 rpm, washed with water, ethanol, and acetone, and dried at 40 °C. Infrared and Mössbauer analysis were used to investigate these changes in the solid material as mentioned previously. Electronic spectra of the supernatants were also taken.

Mössbauer analyses were performed before and after chemical or photochemical treatment of MPSi−NP, whose data were taken in a spectrophotometer in constant acceleration mode setup with a ^{57}Co (Rh) source of gama radiation at room temperature, 110 K, and 20 K. The Mössbauer data were fitted to discrete Lorentzian functions, using the least-squares fitting routine of the NORMOS software package.

Quantitative Measurement of Ferricyanide, Nitroprusside, and Free Cyanide. During the NO release promoted by chemical reduction or light, a quantitative measurement of the products and reagent was done. Ferricyanide and nitroprusside were measured in the supernatant, before and after treatment of the nanoparticles, by electronic spectroscopy, where linear standard curves of nitroprusside (R^2 = 0.993, ABS = 0.133[NP] + 9.7 × 10^{-3}, [NP] = 1 × 10^{-4} M) and ferricyanide were prepared (R^2 = 0.995, linear, ABS = 0.169[Ferricyanide] + 1.8 × 10^{-2}, [Ferricyanide] = 1 × 10^{-4} M). Ferricyanide was measured by using an analytical standard curve prepared in the range of 0.1 to 1.0 mM using its characteristic absorption band at 420 nm.

Free cyanide in solution was measured using a Seal AutoAnalyzer 3 RH (Seal Analytical) by standard methods: 4500 CN^- C (total cyanide after distillation) and 4500 CN^- E (colorimetric method).[23] Once MPSi−NP was removed by centrifugation, total cyanide in the remaining solution was quantified. Briefly, cyanide in the alkaline distillate from previous treatment was converted to cyanogen chloride (CNCl) by reaction with chloramine-T at pH < 8, to prevent any hydrolysis to cyanate (CNO^-) anion. After that reaction, the CNCl species forms a red-blue color with addition of a pyridine−barbituric acid reagent, which is quantified by colorimetry at 575−582 nm.

Vascular Functional Studies. The thoracic aorta of male Wistar rats and guinea pigs and pulmonary arteries of guinea pigs were used for the *ex vivo* studies (n = 7 animals; one vessel from each animal). Rats or guinea pigs were killed by overdose of sodium thiopental (150 mg kg^{-1}) followed by cervical displacement as approved by the Ethic Committee of the Ceará State University (UECE) under the protocol # 2897836/15. The thoracic aorta or pulmonary artery were carefully removed and cut in rings of approximately 4 mm in length. The perivascular adipose tissue was removed from the vessel while being gassed (95% O_2/5% CO_2), and then, it was mounted in a 5 mL organ bath containing Krebs−Henseleit

DOI: 10.1021/acs.molpharmaceut.9b00110
Mol. Pharmaceutics 2019, 16, 2912−2921

solution at 37 °C. After equilibration, the rings were precontracted with phenylephrine (PE, 1 μM) and were placed under a constant 1 g of tension throughout the experimentation, once preliminary results indicated this condition as the optimal tension value. Then, increasing amounts of MPSi−NP (10^{-10} to 10^{-6} M in tissues taken from rats or 10^{-10} to 10^{-5} in tissues taken from guinea pigs) were added. The vasorelaxant effect is measured as percentage of the maximal contraction induced by phenylephrine.

Activation of the Vasodilator-Stimulated Protein (VASP). The level of phosphorylation of Ser239 of VASP is a useful marker for monitoring cGMP-dependent protein kinase activation and signaling. The effects of 1 μM SNP or MPSi−NP compared with the isovolumetric addition of vehicle only (control) were studied. In order to measure the level of phosphorylated VASP, aortic ring samples were homogenized in PBS enriched with Halt Protease Inhibitor Cocktail (1:100; Thermo Scientific, Waltham, MA, USA) and 5 mM EDTA by TissueLyzer (Qiagen, Hilden, Germany). The resulting homogenates were centrifuged at 17 000*g* at 4 °C for 30 min, and the supernatant of this procedure was taken for further procedures. The proteins were resolved by using SDS−PAGE gel electrophoresis. Briefly, aliquots of 50 μg of protein were subjected to SDS−PAGE (10% acrylamide) and transferred to a PVDF membrane at 500 mA overnight using an Hoefer apparatus (Holliston, MA, USA). Thereafter, the membrane was immersed in a TBS-T blocking solution (0.05% Tween 20/0.1 M Tris/0.15 M NaCl, pH 7.5 plus 5% BSA). The membranes were then incubated overnight with the primary antibody for Ser239 of the vasodilator-stimulated phosphoprotein (VASP) (1:1000, Cell Signaling, Danvers, MA, USA), total VASP, or β-actin (1:5000, Sigma) as the internal loading control. The membrane was further incubated for 1 h at room temperature with an anti-rabbit secondary antibody conjugated with alkaline phosphatase. The blot was developed using a chemiluminescence kit (CDP Star, Applied Biosystems) and read by using a Chemidoc XRS+ photo-documentation system (Biorad, Hercules, CA, USA).

Cytotoxicity Assay. This assay was carried out using VERO cells, which were cultured in 24-well dishes containing 1 mL of media per well. The culture growth was performed at 37 °C in 5% CO_2 in a humidified incubator. The basic culture medium consisted of RPMI 1640 (pH 7.2−7.4, Sigma R8758) supplemented with newborn calf serum (2%, NCS) and penicillin and streptomycin (100 μg/mL of each). After 80% of the cells reached confluence, cells were treated with SNP and MPSi−NP at 1, 5, 10, 50, 100, 500, and 1000 μM for 18 h. Cell viability was evaluated by using the trypan blue assay, and for this purpose, 100 cells were counted per treatment in a Neubauer chamber. All of these experiments were done three times.

RESULTS

Characterization of MPSi−NH_2 and MPSi−NP. In the present study, amino groups incorporated in the silica matrix (MPSi−NH_2) originated a positive zeta potential (ζ) value of 20 ± 0.5 mV for this particle. Scanning electron microscopy (SEM) of MPSi−NH_2 shows a spherical shape with a uniform size distribution between 80 and 110 nm (Figure 1a). The N_2 adsorption/desorption isotherms (Figure 1b) of the MPSi−NH_2 exhibited a 2.3 nm porous size and a surface area of 678 $m^2\ g^{-1}$. IR spectra for MPSi−NH_2 and MPSi−NP are shown in Figure 1c, where large bands were observed between 3750−3000 cm^{-1} and at 1650 cm^{-1}, along with other typical bands associated with silica at 480, 920, 1200, and 1100 cm^{-1} and with carbon-modified silica at 1412 cm^{-1}. Interestingly, adsorption of nitroprusside on MPSi−NH_2 caused clear changes in the IR spectrum of the MPSi−NP, where a strong band at 1935 cm^{-1} along with bands at 2026, 2111, 2041, and 661 cm^{-1} were seen (Figure 1c).

In addition to that, Mössbauer analysis was carried out at room temperature, to investigate NP incorporation (Figure 1d, black line). Data analysis showed three subspectra with distinct iron centers. One of those deconvoluted spectra, Figure 1d (blue line), showed an isomeric shift (δ) and a nuclear quadrupole moment (Δ) of ca. −0.09 and 1.53 mm/s. The other two nuclei exhibited δ of 0.54 mm/s (green) and 0.18 mm/s (red line) along with Δ of 0.79 mm/s (green) and 0.00 (red line), respectively (Figure 1d).

Furthermore, we digested MPSi−NP using basic solution and measured the amount of the nitroprusside using UV−vis analysis (Figure 2), which was 323.9 ± 7.55 μmol g^{-1}.

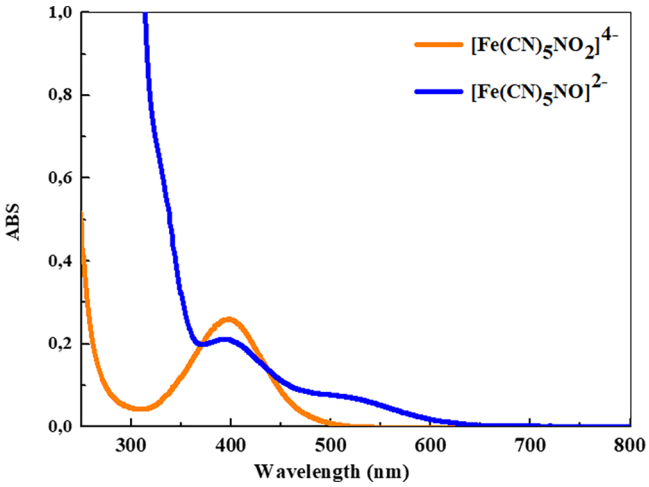

Figure 2. Electronic spectra of nitroprusside (1 mM) (blue line) and in basic media (3 mM NaOH) (orange line).

Mössbauer analysis indicated ∼80% of iron-based compound on this nanoparticle was Prussian blue (PB). So, we investigated if PB was produced in solution during SNP incorporation or afterward. If PB was produced during the process of incorporation of SNP, it might precipitate on the surface of those nanoparticles because of its very low water solubility. However, if it is produced afterward, then it might be found within the matrix in more internal porous structures. Then, to address these hypotheses, PB was chemically synthesized and used dissolved in ethanol solution as our standard material for UV−vis measurements. MPSi−NP was incubated with ethanol solution aiming to extract any PB on the surface, and the supernatant was analyzed. Interestingly, UV−vis measurements did not show any significant amount of PB, indicating it might be produced once SNP binds to the nanoparticles.

NO Release. Aiming to evaluate if MPSi−NP is indeed capable to release nitric oxide under different stimuli, we used light and chemical reducing agents.

Photochemical Release of NO. NO photolabilization from MPSi−NP pellets was carried out using a blue LED (450−495 nm) and monitored by infrared absorption at 1935 cm^{-1}, a band assigned to NO stretching, at room temperature (Figure

DOI: 10.1021/acs.molpharmaceut.9b00110
Mol. Pharmaceutics 2019, 16, 2912−2921

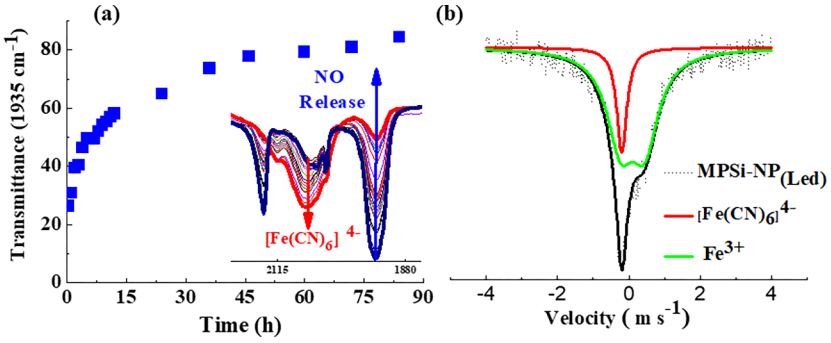

Figure 3. Photorelease of NO using blue LED. (a) IR spectra of NPSi-NP in KBr pellets irradiated with blue LED and (b) Mössbauer spectrum of NPSi-NP after irradiation (96 h) in aqueous dispersion.

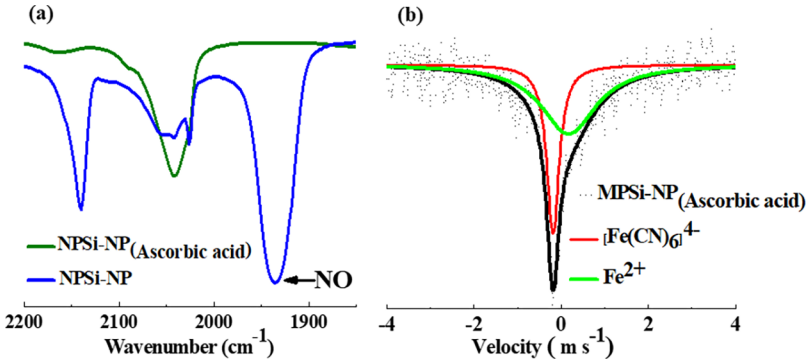

Figure 4. Effect of reducing agents on MPSi−NP. (a) IR and (b) Mössbauer spectra of MPSi−NP after reduction (2 h) with ascorbic acid.

Table 1. Measurement of Free Cyanide Produced during Photochemical and Chemical Treatment of MPSi−NP for NO Release from 100 mg of Dispersed MPSi−NP and 9.5 mg of SNP[a] in 10 mL of PBS

	blue light		ascorbic acid	
	SNP	MPSi−NP	SNP	MPSi−NP
free CN^- (μmol)	30.12 ± 0.021	10.80 ± 0.424	26.60 ± 0.424	21.99 ± 0.1626
relative CN^- released (%)[b]	35.86		82.66	

[a]Identical total amount of SNP used as incorporated on MPSi−NH2. [b]This amount is the percentage of cyanide release by MPSi−NP considering the maximum observed for free SNP as 100% upon that stimulus.

3a). On the basis of these spectra, almost 80% of NO was released from MPSi−NP pellets, after 84 h of light irradiation.

NO photorelease from MPSi−NP was also observed in PBS dispersion, reaching completion within 96 h of incubation as indicated by a Mössbauer spectrum of the photolyzed nanoparticle (Figure 3b). In that spectrum, two nuclei were observed with a doublet at δ = 0.54 mm/s and Δ = 0.79 mm/s and a singlet at δ = 0.18 mm/s. In addition to that, UV−vis analysis of the supernatant showed a characteristic spectroscopic band of ferricyanide at 420 nm (Figure S1), and the quantification shows 25.3 ± 0.6 μmol in 100 mg of MPSi−NP.

In addition to those measurements, the Griess assay was used to validate and quantify the production of nitric oxide.[24] This assay has been used for this purpose in other NO donor systems[25−27] and relies on the aerobic fast conversion of NO to NO_2^-. This assay was performed with free SNP and NPSi-NP in PBS, which were irradiated with blue light, and the supernatant was collected for nitrite measurements. In both samples, nitrite was clearly measured and supporting NO has been released (Figure S2), whereas a quantitative measurement of nitrite produced from NPSi-NP of 335.2 ± 3.7 μmol g^{-1} was obtained after 18 h of light irradiation.

Chemical Release of NO Using Reducing Agent. Aiming to chemically release NO, we employed ascorbic acid as a reducing agent to promote its release from MPSi−NP in aqueous suspension and PBS (Figure 4a). The IR spectra of MPSi−NP before and after chemical reduction were taken showing complete reaction. The Mössbauer spectrum for MPSi−NP, after reduction (Figure 4b), showed that all NP was converted to cyanoferrate species supporting IR measurements. NO release was almost complete within 2 h of reaction. In addition to that, UV−vis analysis of the supernatant after NO release did not show any indication of ferricyanide and ferrocyanide at 420 and 338 nm, respectively (Figure S3).

Cyanide Release. The measurement of cyanide release was conducted using a sample of MPSi−NP dispersed in PBS and pretreated with light or ascorbic acid (Table 1). All values described are relative to a maximum release of cyanide from free SNP upon those stimuli.

Vascular Functional Studies. To evaluate the biological efficiency of the MPSi−NP, we carried out measurements using thoracic aorta and pulmonary arteries. Interestingly, the nanoparticle promoted relaxation on aortic rings from Wistar rats with similar potency to nonmodified SNP, exhibiting a concentration necessary to induce 50% of vasodilation (EC_{50})

DOI: 10.1021/acs.molpharmaceut.9b00110
Mol. Pharmaceutics 2019, 16, 2912−2921

of 26 nM [95% confidence interval of 20−33 nM] (Figure S4), while nonmodified SNP was of 13 nM [95% confidence interval of the 7.9−21 nM]. However, the maximal vasodilation induced by MPSi−NP (177.4 ± 7.1%) was actually higher than the maximal relaxation induced by nonmodified SNP (143.8 ± 9.6%; $P < 0.05$, Student's t test) (Figure 5).

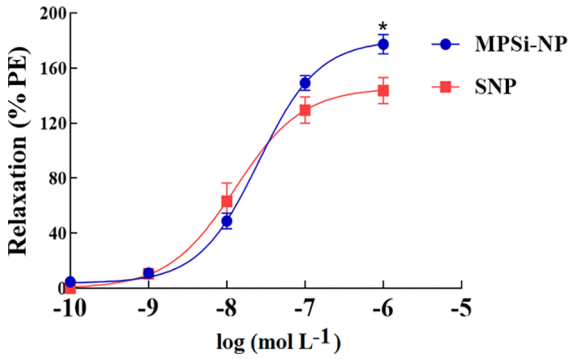

Figure 5. Effect of vasodilation using aorta from Wistar rats and comparison of MPSi−NP (red circles) and free sodium nitroprusside (SNP, blue squares) on the phenylephrine precontracted aortic rings. *$p < 0.05$ vs SNP at the same concentration.

Further investigations using different vascular beds from guinea pigs (i.e., thoracic aorta vs pulmonary arteries) showed MPSi−NP had a similar potency and efficacy in those tissues (Figure 6). The EC_{50} for the vasodilation induced by MPSi−NP in the pulmonary artery was 193 nM [95% confidence interval of 141−264 nM] and in the aorta was 71.2 nM [95% confidence interval of 48−105 nM].

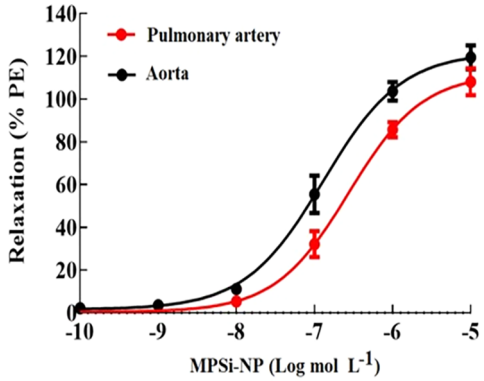

Figure 6. Vasorelaxant effect of MPSi−NP on phenylephrine precontracted aorta or pulmonary arteries taken from guinea pigs. No statistical differences were found.

Activation of Vasodilator-Stimulated Protein (VASP). We investigated the induction of VASP phosphorylation, which can be promoted in a cascade induced by nitric oxide. Interestingly, the ability of MPSi−NP to activate VASP protein by phosphorylation of the Ser239 residue caused by a cGMP-dependent protein kinase was also similar to the effect of nonmodified SNP. The level of phosphorylation of this protein was increased 4-fold by both compounds (Figure 7).

Cytotoxicity Assays. Despite the measurements indicating a decrease in the release of cyanide by MPSi−NP in comparison to free SNP, it cannot ensure biological safety. To preliminarily address any safety use of MPSi−NP, cytotoxicity assay was carried out using kidney epithelial cells (Vero cells). In this assay, SNP and MPSi−NP were used from 1 up to 1000 μM, which was incubated with Vero cells for 18 h before a cell viability assay was performed with trypan blue. The calculated LC_{50} (50% lethal dose) for SNP was 228.5 μM (147.2−354.8 μM) (Figure 8). Unfortunately, we could not estimate the LC_{50} for MSPi-SN using concentrations up to 1000 μM. The maximal decrease in cell viability induced by MPSi−NP was only 13.1 ± 3.2% (Figure 7).

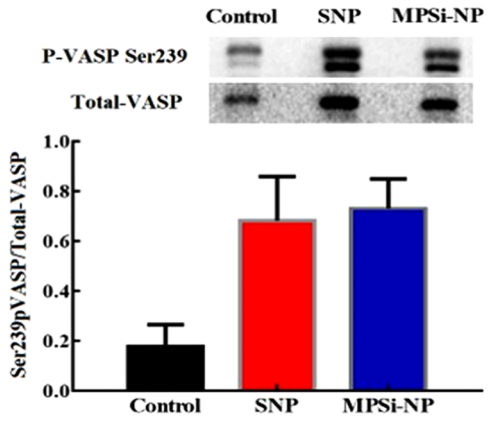

Figure 7. Effect of 1 μM SNP or MPSi−NP compared with the isovolumetric addition of vehicle only (control) in the level of phosphorylation of the serine 239 residue of the protein vasodilator-stimulated phosphoprotein (VASP), a substrate of cGMP-activated protein kinase (PKG). *$p < 0.05$ vs control, Student's t test.

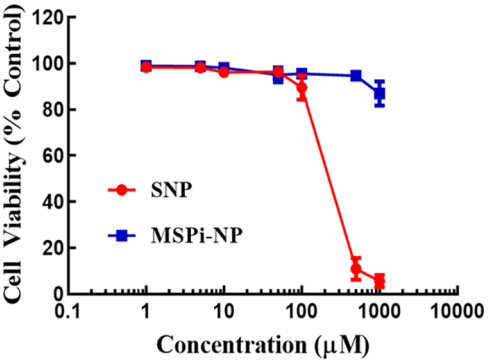

Figure 8. Effects of SNP or MPSi−NP (1, 5, 10, 50, 100, 500, 1000 μM) on the viability of VERO cells. The cells were cultured in 24-well plates until 80% confluence was achieved. The compounds were incubated for 18 h, and the experiments were repeated three times.

DISCUSSION

The MPSi−NH_2 prepared exhibited a zeta potential of +20 ± 0.5 mV, which has been associated with the detergent acid extraction treatment promoted in water. This result was expected based on the fact that the zeta potential reported for nonaminated silica is negative.[28] It is well-known that zeta potential values within a modulus of >30 mV reflect more stable colloidal systems.[29] Although the value obtained in this work is slightly lower than 30 mV, it can still be considered reasonably good and similar to other systems.[30]

The results of N_2 adsorption/desorption isotherms of the MPSi−NH_2 suggest this nanoparticle is indeed a mesoporous material (Figure 1b). In addition to that, IR shows a series of typical bands assigned to silica-based materials, where the

DOI: 10.1021/acs.molpharmaceut.9b00110
Mol. Pharmaceutics 2019, 16, 2912−2921

bands between 3750−3000 cm^{-1} were assigned to O−H of the silanol and water, and the band at 1650 cm^{-1} was assigned to angular vibration of water molecules. The strong bands at 1200 and 1100 cm^{-1} were assigned to asymmetric stretching (υ_{as}) of Si−O−Si, while the bands at 920 and 480 cm^{-1} were assigned to symmetric stretching (υ_{sim}) of Si−O−Si and angular deformation (δ) of O−Si−O, respectively.[31,32] The Si−C bond stretching was also observed at 1412 cm^{-1}. The bands at 1535 and 1552 cm^{-1} were assigned to $SiO^{-}\cdots NH_3^{+}$ interactions.[33] Interestingly, once this nanoparticle was modified with nitroprusside (MPSi−NP), a remarkable change in IR spectrum was noticed, particularly the appearance of a strong band at 1935 cm^{-1} assigned to NO. Additionally, other bands observed at 2026, 2111, and 2041 cm^{-1} were assigned to cyanide stretching, along with Fe−C (δ) at 661 cm^{-1}, fully reinforcing the presence of nitroprusside on the nanoparticle.[34,35]

Mössbauer analysis indicated three distinct iron centers in MPSi−NP, whereas only one iron center was initially expected because of the nitroprusside itself ($[Fe^{II}(CN)_5NO]^{2-}$). The first nuclei with an isomeric shift (δ) and nuclear quadrupole moment (Δ) of ca. −0.09 and 1.53 mm/s, respectively, was indeed assigned to the nitroprusside ions ($[Fe^{II}(CN)_5NO]^{2-}$), in comparison to free sodium nitroprusside standard (SNP) (δ = 0.00 mm/s and Δ = 1.65 mm/s) (Figure S5). The microenvironment can slightly alter Mössbauer parameters as noticed by the effect of counterions on nitroprusside ($K_2[Fe^{II}(CN)_5NO]$, δ = 0.07 mm/s and Δ = 1.74 mm/s; $Li_2[Fe^{II}(CN)_5NO]$, δ = 0.05 mm/s and Δ = 1.61 mm/s).[36] The decrease of δ and Δ values for nitroprusside on the nanoparticle might suggest a greater electron density around the iron nucleus that may be influenced by the immediate vicinity. Nonetheless, this result indicated SNP was successfully incorporated on the MPSi−NH_2. Furthermore, the other two nuclei illustrated by red (δ = 0.54 mm/s, Δ = 0.79 mm/s) and green (δ = 0.18 mm/s, Δ = 0.00) lines, Figure 1d, were fully consistent with the Prussian blue (PB) complex ($Fe^{III}_4[Fe^{II}(CN)_6]_3$), which contains two distinct iron centers.[37] This latter species is a well-known compound that can be formed by decomposition of SNP, most likely produced here because of the acid−base properties of the nanoparticle. Besides that, Mössbauer semiquantitative analysis indicated that ∼20% of the total iron nuclei present in MPSi−NP is due to NP and the remaining to ($Fe^{III}_4[Fe^{II}(CN)_6]_3$) complex.

A quantitative analysis of nitroprusside incorporated on these nanoparticles showed a quite large value (323.9 ± 7.6 μmol g^{-1}, Figure 2), particularly if compared to other reports that use SNP and other NO release systems (Table 2). Despite that, Mossbauer analysis indicated the largest amount of iron-based material in the nanoparticle, ∼80% was due to Prussian blue (PB, ($Fe^{III}_4[Fe^{II}(CN)_6]_3$)). Interestingly, our study suggested no precipitation of PB onto MPSi−NP took place during incorporation of SNP, and PB was likely produced within and after SNP bound to silica. However, PB is highly insoluble, considered nontoxic, well-tolerated, and difficult for the digestive tract to absorb.[38] Indeed, since 2003, PB has been an FDA-approved drug used for the treatment of internal contamination with radioactive ^{137}Cs and ^{201}Tl, sold as Radiogardase. It is important to further remark that our large incorporation of SNP on silica nanoparticle was almost 300-fold higher than others.[18] Was achieved this by the detergent removal acidic treatment. On the other hand, this treatment led to partial decomposition of bound SNP and formation of Prussian blue, a trade-off necessary for large incorporation of SNP.

Table 2. Comparison of Different NO Release Systems Found in the Literature

material	loading of NO (mol g^{-1})	measurements method	reference
$[Si(CH_2)_3(isn)Ru(NH_3)_4(NO)]^{3+}$	1.3×10^{-4}	Ru elemental analysis	39
$Si(CH_2)_3NH_2$[SNP]	9.6×10^{-7}	Fe elemental analysis	18
$Si(CH_2)_3NH_2$[SNP]	3.3×10^{-4}	UV−vis	this work
Alg300-DETA/NO	6.5×10^{-4}	chemiluminescence	40
MethylQA/NO	3.0×10^{-4}	chemiluminescence	41

Photorelease of NO from MPSi−NP pellets was achieved using either blue light or chemical reducing agents, which reinforced that the nitroprusside was incorporated and capable of releasing NO. The Mössbauer spectrum of the light-irradiated nanoparticle showed only one subspectrum assigned to the Prussian blue complex ($Fe^{III}_4[Fe^{II}(CN)_6]_3$) with a doublet at δ = 0.54 mm/s and Δ = 0.79 mm/s and a singlet at δ = 0.18 mm/s (Figure 3b). In addition to that, an electronic transition band with a maximum at 420 nm was also noticed in the supernatant of the light-treated dispersion (Figure S1), which is characteristic of the ferricyanide ion ($[Fe^{III}(CN)_6]^{3-}$). The production of ferricyanide supports the release of NO· due to the photoreduction of NO^+ promoted by Fe^{II}, yielding an intermediate of $[Fe^{III}(CN)_5(H_2O)]^{2-}$ (eq 1).

$$[Fe^{II}(CN)_5(NO^+)]^{2-} + H_2O \rightarrow [Fe^{III}(CN)_5(H_2O)]^{2-} + NO\cdot \quad (1)$$

Other authors[35] have showed the formation of mixed valence complexes, including Prussian blue, during decomposition of nitroprusside (eq 2).

$$7[Fe^{II}(CN)_5(NO)]^{3-} \rightarrow Fe_4^{III}[Fe^{II}(CN)_6]_3 + 17CN^- + 7NO \quad (2)$$

The use of Griess reagent to detect and quantify nitrite (NO_2^-), a well-known final species of NO in aerobic solution, was successfully employed. Indeed, a side-by-side experiment using free SNP and MPSi−NP in PBS fully supported that there is a release of NO. Actually, the quantitative measurement of total NO_2^- produced by MPSi−NP, after 18 h of light irradiation, was 335.2 ± 3.7 μmol g^{-1}, which is in close agreement to the total amount of nitroprusside incorporated as measured by UV−vis (323.9 ± 7.6 μmol g^{-1}).

In addition to that, chemical reduction of the nanoparticle in water and PBS also showed a fast and efficient release of NO as monitored by IR and supported by Mössbauer spectrum (Figure 3). This is indeed a likely route for the biological release of NO, supporting that this nanoparticle as a biologically active material.

One of the major drawbacks in the clinical use of nitroprusside remains the significant amount of cyanide released, an issue minimized by the coadministration of some antidotes such as thiosulfate. Here, we investigated whether MPSi−NP would release less cyanide. A significant difference in the amount of free CN^- released depending on the method used to induce NO release was observed. Once we used photochemical induction, we observed 35.86% of cyanide release, while chemical induction using ascorbic acid resulted in 82.66% (Table 1). The larger release of cyanide when using ascorbic acid might be due to a competition between cyanide and ascorbate ions for the surface of the material. Indeed, the

DOI: 10.1021/acs.molpharmaceut.9b00110
Mol. Pharmaceutics 2019, 16, 2912−2921

IR spectrum of the MPSi−NP nanoparticle treated with ascorbic acid showed a characteristic stretching band of the carbonyl group (C=O) of the ascorbic acid (Figure 4a) shifted from 1754 to 1735 cm^{-1} (Figure S6), suggesting an interaction of the ascorbate with the silica matrix.[13] This data suggests that ~64% of cyanide is not released from the nanoparticle once compared to an identical sample of free nitroprusside. We should remark that 100% of cyanide release does not mean all five cyanides of SNP, since some final products also contain strongly bound cyanide such as the ferricyanide species. Nevertheless, the value of free cyanide released is significantly smaller and places a great expectation for the safer use of this anchored SNP.

We carried out a series of biological assays using the MPSi−NP in comparison to free SNP (Figures 5 and 6). In all of these studies, either using thoracic aorta and pulmonary arteries from two distinct animal models, Wistar rats or guinea pigs, we observed great similarity in the potency and efficacy in those tissues (Figure 5) with concentrations at the nanomolar range. Actually, in Wistar rats, the potency of our nanoparticles was even higher than that of free SNP, opening avenues for its potential use to treat both systemic as well as pulmonary hypertension. These results along with our chemical studies support an efficient NO release as previously indicated, enabling the use of anchored SNP with lower cyanide issue.

Furthermore, VASP phosphorylation was also investigated. This measurement is very useful to monitor the effect of so-called antiplatelet drugs that reduce platelet reactivity. The regulation of this biological activity can be used to prevent stent thrombosis, strokes, and heart attacks in patients at risk of these problems. Thus, we investigated the induction of VASP phosphorylation, which can be promoted in a cascade induced by nitric oxide. Interestingly, the ability of MPSi−NP to activate VASP protein by phosphorylation of the Ser239 residue caused by a cGMP-dependent protein kinase, was also similar to the effect of free SNP, supporting the analogous efficiency of the nanoparticle (Figure 7), providing other opportunities of biological applications.

Beyond the NO-dependent biological activities described above, the cytotoxicity measurements of MPSi−NP done in mammalian cells provided further support to a safer use of this nanomaterial in comparison to free SNP (Figure 8). It is interesting to point out that vasodilation effects occurred at nanomolar range in close similarity for both MPSi−NP and SNP, but their cytotoxicities were very distinct. Despite this, we were unable to measure LC_{50} for MPSi−NP, but we can ensure it is at least 5-fold higher than free SNP. These results also reinforced our expectation that cyanoferrate species, released from MPSi−NP, might not contribute significantly to any further toxicity. Indeed, human red blood cells rapidly convert extracellular ferricyanide ($[Fe^{III}(CN)_6]^{3-}$) into ferrocyanide ($[Fe^{II}(CN)_6]^{4-}$). However, $[Fe^{III}(CN)_6]^{3-}$ has a quite low toxicity, with LC_{50} in rats of 1600 to 3200 mg kg^{-1} body weight when administered orally. After absorption into the bloodstream, ferrocyanide appears to be eliminated via the glomeruli and not excreted via renal tubules,[42] which makes this nanoparticle a promising strategy to reduce the toxicity of SNP. Moreover, we should note that this nanoparticle might have quite different pharmacokinetic and pharmacodynamics from the free SNP. Thus, it could open opportunities for wider and newer uses of this anchored SNP including topical therapy.

CONCLUSION

Our synthetic strategy to make functionalized silica nanoparticles was successful with the incorporation of sodium nitroprusside up to 323.9 ± 7.6 μmol g^{-1}, 300-fold more than other silica-based materials. Remarkably, we also noticed a minor release of cyanide or even SNP, despite the fact that its full biological effect was maintained based on the NO release. Indeed, the EC_{50} for vasodilation was very close to those of free NP, supporting its full efficiency despite being strongly anchored to the nanoparticle. The similar efficiency of MPSi−NP to induce vasodilation in aorta and pulmonary arteries shows a great potential to treat pulmonary and systemic hypertension by decreasing cardiac preload and pulmonary arterial pressure. Nonetheless, the lower cytotoxicity for this nanoparticle found in mammalian cells reinforces its promising use. In addition to that, the high levels of NP on silica nanoparticles can open opportunities in a variety of other applications, even for topical use, which is not suitable for SNP, a very water-soluble compound easily washed out on the skin.

ASSOCIATED CONTENT

Supporting Information

The Supporting Information is available free of charge on the ACS Publications website at DOI: 10.1021/acs.molpharmaceut.9b00110.

Figures S1 to S6: UV−vis spectrum of nanoparticle treated with light; UV−vis spectra of Griess tests; UV−vis spectrum of nanoparticle treated with ascorbic acid; effect of vasodilation using aorta; Mössbauer spectra of SNP; IR of nanoparticle after ascorbic acid treatment (PDF)

AUTHOR INFORMATION

Corresponding Authors

*E-mail: elisane@ufc.br; Phone: +55 85 33669052. (E.L.)
*E-mail: eduardohss@dqoi.ufc.br; Phone: +55 85 33669938. (E.H.S.S.)

ORCID

T. S. Ribeiro: 0000-0001-9223-3730
Eduardo H. S. Sousa: 0000-0002-0007-8452
Elisane Longhinotti: 0000-0002-4782-6905

Notes

The authors declare no competing financial interest.

ACKNOWLEDGMENTS

E.L. (CNPq researcher fellowship #306896/2018-4), E.H.S.S. (CNPq researcher fellowship #308383/2018-4, Universal 403866/2016-2), and L.G.F.L. (CNPq researcher fellowship #303355/2018-2, PRONEX PR2 0101-00030.01.00/15, and CAPES (23038.008968/2012-87)), are thankful to CNPq, FUNCAP, and CAPES (PROEX 23038.000936/2018-46 and CAPES/Print/UFC) for financial support. We greatly acknowledge the Companhia Siderúrgica do Pecém (CSP) for cyanide analysis and the Central Analítica UFC/CT-INFRA/MCTI-SISNANO/Pró-Equipamentos CAPES.

REFERENCES

(1) Hottinger, D. G.; Beebe, D. S.; Kozhimannil, T.; Prielipp, R. C.; Belani, K. G. Sodium Nitroprusside in 2014: A Clinical Concepts Review. *J. Anaesthesiol. Clin. Pharmacol* **2014**, *30* (4), 462−471.

DOI: 10.1021/acs.molpharmaceut.9b00110
Mol. Pharmaceutics 2019, 16, 2912−2921

(2) Johanning, R. J.; Zaske, D. E.; Tschida, S. J.; Johnson, S. V.; Hoey, L. L.; Vance-Bryan, K. A Retrospective Study of Sodium Nitroprusside Use and Assessment of the Potential Risk of Cyanide Poisoning. *Pharmacotherapy* **1995**, *15* (6), 773−777.
(3) Wu, S. C.; Lu, C. Y.; Chen, Y. L.; Lo, F. C.; Wang, T. Y.; Chen, Y. J.; Yuan, S. S.; Liaw, W. F.; Wang, Y. M. Water-Soluble Dinitrosyl Iron Complex (DNIC): A Nitric Oxide Vehicle Triggering Cancer Cell Death via Apoptosis. *Inorg. Chem.* **2016**, *55* (18), 9383−9392.
(4) Ke, C. H.; Chen, C. H.; Tsai, M. L.; Wang, H. C.; Tsai, F. Te; Chiang, Y. W.; Shih, W. C.; Bohle, D. S.; Liaw, W. F. $\{Fe(NO)_2\}^9$ dinitrosyl Iron Complex Acting as a Vehicle for the NO Radical. *J. Am. Chem. Soc.* **2017**, *139* (1), 67−70.
(5) Pulukkody, R.; Chupik, R. B.; Montalvo, S. K.; Khan, S.; Bhuvanesh, N.; Lim, S. M.; Darensbourg, M. Y. Toward Biocompatible Dinitrosyl Iron Complexes: Sugar-Appended Thiolates. *Chem. Commun.* **2017**, *53* (6), 1180−1183.
(6) Ford, P. C. Polychromophoric Metal Complexes for Generating the Bioregulatory Agent Nitric Oxide by Single- and Two-Photon Excitation. *Acc. Chem. Res.* **2008**, *41* (2), 190−200.
(7) Eroy-Reveles, A. A.; Hoffman-Luca, C. G.; Mascharak, P. K. Formation of a Triply Bridged μ-Oxo Diiron(III) Core Stabilized by Two Deprotonated Carboxamide Groups upon Photorelease of NO from a $(Fe-NO)^6$ iron Nitrosyl. *J. Chem. Soc. Dalt. Trans* **2007**, *2* (45), 5268−5274.
(8) Holanda, A. K. M.; da Silva, F. O. N.; Carvalho, I. M. M.; Batista, A. A.; Ellena, J.; Castellano, E. E.; Moreira, Í. S.; Lopes, L. G. F. Crystal Structure, Electrochemical and Photochemical Studies of the Trans-$[Fe(Cyclam)(NO)Cl]Cl_2$ complex (Cyclam = 1,4,8,11-Tetraazacyclotetradecane). *Polyhedron* **2007**, *26* (16), 4653−4658.
(9) Bose, R. J. C.; Lee, S.; Park, H. Biofunctionalized Nanoparticles: An Emerging Drug Delivery Platform for Various Disease Treatments. *Drug Discovery Today* **2016**, *21* (8), 1303−1312.
(10) Farooq, A.; Shukur, A.; Astley, C.; Tosheva, L.; Kelly, P.; Whitehead, D.; Azzawi, M. Titania Coating of Mesoporous Silica Nanoparticles for Improved Biocompatibility and Drug Release within Blood Vessels. *Acta Biomater.* **2018**, *76*, 208−216.
(11) Poonia, N.; Lather, V.; Pandita, D. Mesoporous Silica Nanoparticles: A Smart Nanosystem for Management of Breast Cancer. *Drug Discovery Today* **2018**, *23* (2), 315−332.
(12) Pereira, C.; Araújo, F.; Granja, P.; Santos, H.; Sarmento, B. Targeting Membrane Transporters and Receptors as a Mean to Optimize Orally Delivered Biotechnological Based Drug through Nanoparticle Delivery Systems. *Curr. Pharm. Biotechnol.* **2014**, *15*, 650−658.
(13) Moulari, B.; Beduneau, A.; Pellequer, Y.; Lamprecht, A. Nanoparticle Targeting to Inflamed Tissues of the Gastrointestinal Tract. *Curr. Drug Delivery* **2013**, *10*, 9−17.
(14) Yang, Y.; Nie, D.; Liu, Y.; Yu, M.; Gan, Y. Advances in Particle Shape Engineering for Improved Drug Delivery. *Drug Discovery Today* **2019**, *24* (2), 575−583.
(15) Deligey, F.; Bouguet-Bonnet, S.; Doudouh, A.; Marande, P.; Schaniel, D.; Gansmüller, A. Bridging Structural and Dynamical Models of a Confined Sodium Nitroprusside Complex. *J. Phys. Chem. C* **2018**, *122*, 21883−21890.
(16) da Silva, F. O. N.; Gomes, E. C. C.; Francisco, T. S.; Holanda, A. K. M.; Diógenes, I. C. N.; de Sousa, E. H. S.; Lopes, L. G. F.; Longhinotti, E. NO Donors Cis -$[Ru(Bpy)_2(L)NO]^{3+}$ and $[Fe(CN)(L)NO]^-$ Complexes Immobilized on Modified Mesoporous Silica Spheres. *Polyhedron* **2010**, *29* (18), 3349−3354.
(17) Wei, F.; Hou, Q.; Yang, J. Y.; Zhu, J. H. Multifunctional NO-Delivery Vessel Derived from Aminopropyl-Modified Mesoporous Zeolites. *J. Colloid Interface Sci.* **2011**, *356*, 526−535.
(18) Farooq, A.; Tosheva, L.; Azzawi, M.; Whitehead, D. Journal of Colloid and Interface Science Real-Time Observation of Aortic Vessel Dilation through Delivery of Sodium Nitroprusside via Slow Release Mesoporous Nanoparticles. *J. Colloid Interface Sci.* **2016**, *478*, 127−135.
(19) Rostamian, R.; Najafi, M.; Rafati, A. A. Synthesis and Characterization of Thiol-Functionalized Silica Nano Hollow Sphere as a Novel Adsorbent for Removal of Poisonous Heavy Metal Ions from Water: Kinetics, Isotherms and Error Analysis. *Chem. Eng. J.* **2011**, *171* (3), 1004−1011.
(20) Barrett, E. P.; Joyner, L. G.; Halenda, P. P. The Determination of Pore Volume and Area Distributions in Porous Substances. I. Computations from Nitrogen Isotherms. *J. Am. Chem. Soc.* **1951**, *73* (2), 373−380.
(21) Swinehart, B. Y. J. H.; Rock, P. A. The Equilibrium and Kinetic Properties of the Aqueous Hydroxide-Nitroprusside System. *Inorg. Chem.* **1966**, *5* (4), 573−576.
(22) Butler, A. R.; Glidewell, C. Recent Chemical Studies of Sodium Nitroprusside Relevant to Its Hypotensive Action. *Chem. Soc. Rev.* **1987**, *16*, 361−380.
(23) Greenberg, A. E., Clesceri, L. S., Eaton, A. D., Franson, M. H., Eds. *Standard Methods: For the Examination of Water and Wastewater*, 18th ed.; American Public Health Association, American Water Works Association, and Water Environment Federation, 1992.
(24) Tsikas, D. Analysis of nitrite and nitrate in biological fluids by assays based on the Griess reaction: Appraisal of the Griess reaction in the l-arginine/nitric oxide area of research. *J. Chromatogr. B: Anal. Technol. Biomed. Life Sci.* **2007**, *851*, 51−70.
(25) Ullrich, T.; Oberle, S.; Abate, A.; Schröder, H. Photoactivation of the nitric oxide donor SIN-1. *FEBS Lett.* **1997**, *406*, 66−68.
(26) Akl, J.; Sasaki, I.; Lacroix, P. G.; Malfant, I.; Mallet-Ladeira, S.; Vicendo, P.; Farfán, N.; Santillan, R. *Dalton T.* **2014**, *43*, 12721−12723.
(27) Fan, J.; He, Q.; Liu, Y.; Zhang, F.; Yang, X.; Wang, Z.; Lu, N.; Fan, W.; Lin, L.; Niu, G.; He, N.; Song, J.; Chen, X. Light-Responsive Biodegradable Nanomedicine Overcomes Multidrug Resistance via NO-Enhanced Chemosensitization. *ACS Appl. Mater. Interfaces* **2016**, *8* (22), 13804−13811.
(28) Suteewong, T.; Sai, H.; Cohen, R.; Wang, S.; Bradbury, M.; Baird, B.; Gruner, S. M.; Wiesner, U. Highly Aminated Mesoporous Silica Nanoparticles with Cubic Pore Structure. *J. Am. Chem. Soc.* **2011**, *133*, 172−175.
(29) Wang, P.; Keller, A. A. Natural and Engineered Nano and Colloidal Transport: Role of Zeta Potential in Prediction of Particle Deposition. *Langmuir* **2009**, *25* (14), 6856−6862.
(30) Slowing, I.; Trewyn, B. G.; Lin, V. S. Effect of Surface Functionalization of MCM-41-Type Mesoporous Silica Nanoparticles on the Endocytosis by Human Cancer Cells. *J. Am. Chem. Soc.* **2006**, *128*, 14792−14793.
(31) Vansant, E. F.; Van Der Voort, P.; Vrancken, K. C. *Characterization and Chemical Modification of the Silica Surface*; Elsevier, 1995.
(32) Innocenzi, P. Infrared Spectroscopy of Sol-Gel Derived Silica-Based Films: A Spectra-Microstructure Overview. *J. Non-Cryst. Solids* **2003**, *316* (2−3), 309−319.
(33) Okabayashi, H.; Shimizu, I.; Nishio, E.; Connor, C. J. O. Diffuse Reflectance Infrared Fourier Transform Spectral Study of the Interaction of 3-Aminopropyltriethoxysilane on Silica Gel. Behavior of Amino Groups on the Surface. *Colloid Polym. Sci.* **1997**, *275*, 744−753.
(34) Schuy, A.; Woike, T.; Schaniel, D. J. D. Photoisomerisation in Single Molecules of Nitroprusside Embedded in Mesopores of Xerogels. *J. Sol-Gel Sci. Technol.* **2009**, *50*, 403−408.
(35) Shishido, S. M.; De Oliveira, M. G. Photosensitivity of Aqueous Sodium Nitroprusside Solutions: Nitric Oxide Release versus Cyanide Toxicity. *Prog. React. Kinet. Mech.* **2001**, *26* (2−3), 239−261.
(36) Goel, P. S.; Garg, A. N. Mossbauer Spectroscopic Studies of the Alkali Metal and Transition Metal Nitroprussides. *Inorg. Chem.* **1971**, *10* (7), 1344−1347.
(37) Rasmussen, P. G.; Meyers, E. A. An Investigation of Prussian Blue Analogues by Mössbauer Spectroscopy and Magnetic Susceptibility. *Polyhedron* **1984**, *3* (2), 183−190.
(38) Pearce, J. Studies Of Any Toxicological Effects of Prussian Blue Compounds in Mammals−A Review. *Food Chem. Toxicol.* **1994**, *32* (6), 577−582.

DOI: 10.1021/acs.molpharmaceut.9b00110
Mol. Pharmaceutics 2019, 16, 2912−2921

(39) Doro, F. G.; Rodrigues-Filho, U. P.; Tfouni, E. A Regenerable Ruthenium Tetraammine Nitrosyl Complex Immobilized on a Modified Silica Gel Surface: Preparation and Studies of Nitric Oxide Release and Nitrite-to-NO Conversion. *J. Colloid Interface Sci.* **2007**, *307*, 405−417.
(40) Ahonen, M. J. R.; Suchyta, D. J.; Zhu, H.; Schoenfisch, M. H. Nitric Oxide-Releasing Alginates. *Biomacromolecules* **2018**, *19* (4), 1189−1197.
(41) Carpenter, A. W.; Worley, B. V.; Slomberg, D. L.; Schoenfisch, M. H. Dual Action Antimicrobials: Nitric Oxide Release from Quaternary Ammonium-Functionalized Silica Nanoparticles. *Biomacromolecules* **2012**, *13* (10), 3334−3342.
(42) Liu, Z.; Sun, M.; Zhao, H.; Zhao, M. Acute Self-Induced Poisoning with Sodium Ferrocyanide and Methanol Treated with Plasmapheresis and Continuous Renal Replacement Therapy Successfully. *Medicine (Philadelphia, PA, U. S.)* **2015**, *94* (21), e890.

DOI: 10.1021/acs.molpharmaceut.9b00110
Mol. Pharmaceutics 2019, 16, 2912−2921